Scanning Noise Microscopy on Graphene Devices

Moon Gyu Sung,[†,#] Hyungwoo Lee,[†,#] Kwang Heo,[‡] Kyung-Eun Byun,[†] Taekyeong Kim,[†] David H. Seo,[⊥] Sunae Seo,[⊥,¶] and Seunghun Hong[†,‡,§,*]

[†]Department of Physics and Astronomy, [‡]Interdisciplinary Program in Nano-Science and Technology, and [§]Department of Biophysics and Chemical Biology (WCU Program), Seoul National University, Seoul 151-747, Korea, [⊥]Semiconductor Devices Laboratory, Samsung Advanced Institute of Technology, Yongin-Si, Gyeonggi-do 446-712, Korea, and [¶]Department of Physics, Sejong University, Seoul, 143-747, Korea. [#]These authors contributed equally to this work.

ABSTRACT We developed a scanning noise microscopy (SNM) method and demonstrated the nanoscale noise analysis of a graphene strip-based device. Here, a Pt tip made a direct contact on the surface of a nanodevice to measure the current noise spectrum through it. Then, the measured noise spectrum was analyzed by an empirical model to extract the noise characteristics only from the device channel. As a proof of concept, we demonstrated the scaling behavior analysis of the noise in graphene strips. Furthermore, we performed the nanoscale noise mapping on a graphene channel, allowing us to study the effect of structural defects on the noise of the graphene channel. The SNM method is a powerful tool for nanoscale noise analysis and should play a significant role in basic research on nanoscale devices.

KEYWORDS: atomic force microscopy · scanning noise microscopy · low-frequency noise · graphene strip · nanodevice

In the area of nanoscale device research, various scanning probe microscopy (SPM) methods have been a workhorse for a device analysis because they provide nanoscale mapping of the electronic properties of the components in a nanodevice and thus enable versatile analyses of the device characteristics using only a *single* device.[1−15] For example, conducting atomic force microscopy (CAFM) is a powerful technique to measure electric currents for characterizing conductivity variations in nanoscale channels.[6−10] With Kelvin probe force microscopy, the work function variation on the surfaces of nanodevices can be observed. On the other hand, as the dimension and the operating voltage of modern electronic devices are reduced, its low-frequency noise is becoming a critical parameter determining the device performance.[16−20] Especially, 1/*f* noise can be a significant problem in the devices based on nanomaterials such as graphene,[21−28] carbon nanotubes,[29−31] and nanowires.[32,33] In previous works, noise characteristics of various devices have been analyzed through the scaling behavior obtained from the noise measurement of *multiple* devices with different resistance values.[34−41] However, the fabrication of multiple devices for such noise analysis can be a labor-intensive work. Until now, SPM strategies have not been applied for nanodevice noise analysis.

Herein, we developed a scanning noise microscopy (SNM) method and applied it for the noise analysis of a graphene strip-based device. In the SNM method, a platinum (Pt) tip made a direct contact on the surface of a nanodevice to measure the current noise spectrum through it. Then, the measured noise spectrum was analyzed by an empirical model to extract the noise characteristics of the device channel. As a proof of concept, we applied the SNM method for obtaining the scaling behavior of the noises in graphene channels using a *single* sample, resulting in a similar result as previous works using *multiple* device samples with different channel resistances.[39] Furthermore, we demonstrated a simultaneous mapping of noise characteristics as well as the topography and the current images of a graphene channel around a defect. The SNM method is a simple but powerful strategy for noise analysis and mapping of nanodevices and should play a significant role in the basic researches and the applications of nanoscale devices.

RESULTS AND DISCUSSION

Figure 1a illustrates a schematic diagram depicting our method to prepare graphene strips with pristine surfaces for the SNM analysis. A detailed process can be found in the Methods section. First, a graphene sheet grown by the chemical vapor deposition method was transferred onto a clean SiO_2 substrate (oxide thickness ≈ 1000 Å).[42,43] Using a conventional photolithography method, photoresist (PR) was patterned on the graphene surface.[44,45] The conducting polymer, polypyrrole, was deposited on the

* Address correspondence to seunghun@snu.ac.kr.

Received for review June 10, 2011 and accepted September 27, 2011.

Published online October 06, 2011 10.1021/nn202135g

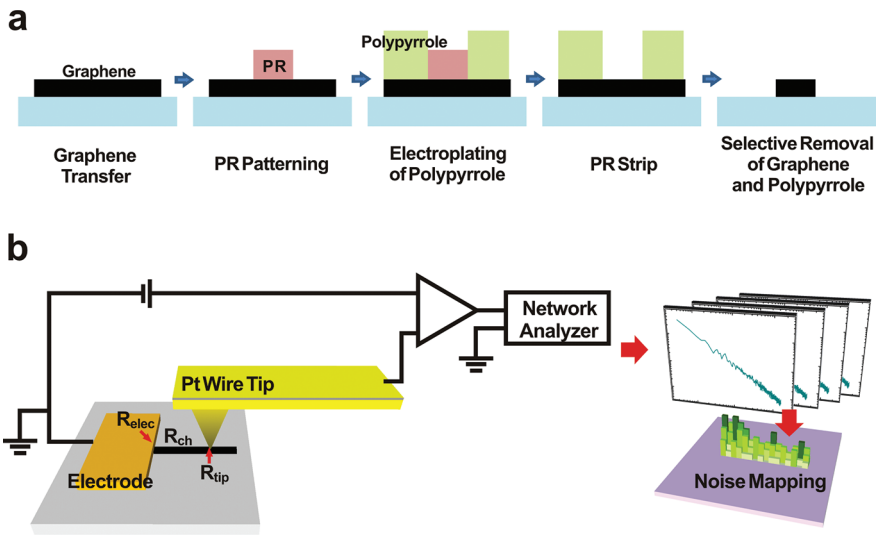

Figure 1. Schematic diagram depicting experimental procedures. (a) Fabrication process of graphene strips. The graphene sheet was transferred onto the SiO_2 substrate. PR patterns were generated on the graphene surface *via* photolithography. The conducting polymer was deposited on the graphene surface by electrochemical deposition. Conducting polymer and underlying graphene layer were eliminated selectively by shaking the substrate in DI water. Finally, the PR layer was removed, resulting in pristine graphene strips. (b) Experimental setup for scanning noise microscopy based on conducting AFM. A Pt tip made a direct contact with graphene strips, and the electrical current through the tip was measured as a conducting AFM signal. For scanning noise microscopy analysis, the power spectral density (PSD) of the measured current was obtained using a network analyzer.

PR-patterned graphene surface by the electrochemical deposition. Then, PR was removed with acetone, leaving only polypyrrole patterns on the graphene surface. The substrate was stirred in deionized water so that the conducting polymer and the underlying graphene strip were mechanically detached off from the substrate, leaving graphene strip patterns. It should be noted that since the PR layer did not go through a high-temperature step in our process, it could be easily removed without leaving a residual film on graphene strips. Thus, the surface of the graphene strips was accessible for electrical contact by an external probe during the SNM analysis.

Figure 1b shows the experimental setup of a SNM based on a conducting AFM. Here, a Pt tip installed on the conducting AFM (XE-70, Park Systems) made a direct contact with a graphene strip surface for the measurement of a current noise spectrum. Note that, to achieve a stable electrical contact, we utilized a Pt tip (25Pt300B, Park Systems) as a probe instead of commonly used metal-coated tips of which a metal coating was peeled easily at the end of the tip during the scanning.[46,47] After the Pt tip made a contact with the surface, a sample bias voltage was applied between an Au electrode and the Pt tip (DS345 function generator, Stanford Research Systems) and the electric currents from the Pt tip to the graphene strip were measured. The measured currents were converted to amplified voltage signals by a low-noise preamplifier (SR570, Stanford Research Systems). Subsequently, the noise power spectral density (PSD) of the signals was measured by a FFT network analyzer (SR770, Stanford Research Systems). Finally, the measured noise spectrum was analyzed using an empirical model to obtain the noise characteristics of the graphene strip channel only. The noise characteristic maps of the graphene strip were obtained by scanning the Pt tip on the graphene strip surface in *x* and *y* directions during the measurement. Since the SNM method is compatible with the conducting AFM mode, we can also obtain topography and current images simultaneously during the SNM operation.

Figure 2a,b are the optical image and the contact-mode AFM topography image of graphene strips, respectively. The graphene strip exhibited clear edges without significant residual contaminations on its surface. The width and the height of the graphene strip were measured as 6.6 μm and 6.6 nm, respectively. The results indicate that our patterning method using polypyrrole allowed us to prepare pristine graphene strips on a SiO_2 substrate.

Figure 2c shows the map of the currents flowing through the graphene strip. The electric current image of the graphene strip was measured at a sample bias of 2 V using a Pt tip. The electric current image of the graphene strip is well matched with the topography image, and it shows a very uniform surface. These results indicate the graphene strip prepared by our fabrication method (Figure 1a) had an *electrically clean* surface. On the other hand, we could not measure current images from the graphene strip fabricated by the oxygen plasma etching method (Figure S1 in Supporting Information).[48−51] Presumably, the oxygen plasma etching process left residual contaminations such as thermally hardened photoresist on graphene, blocking the electrical contact with the Pt tip.[48−51]

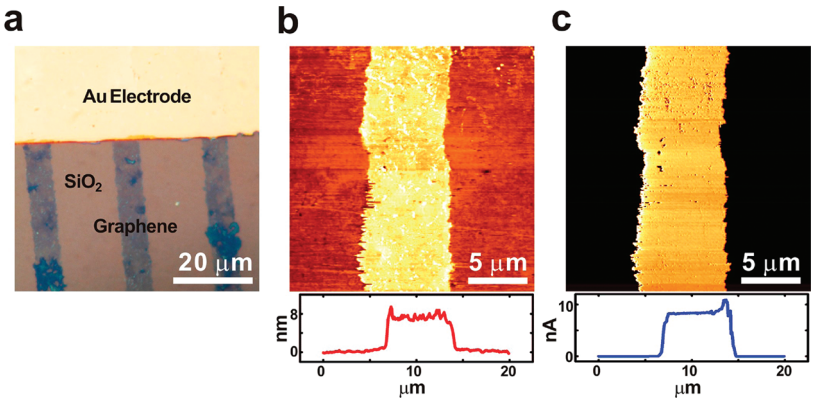

Figure 2. Microscopy images of pristine graphene patterns: (a) optical microscopy image of graphene patterns; (b) contact-mode AFM topography image of graphene strips. The height and width of the graphene strip were measure as 6.6 nm and 6.6 μm, respectively; (c) current image on the graphene strip taken by the conducting AFM. The current range of the image was 10 nA.

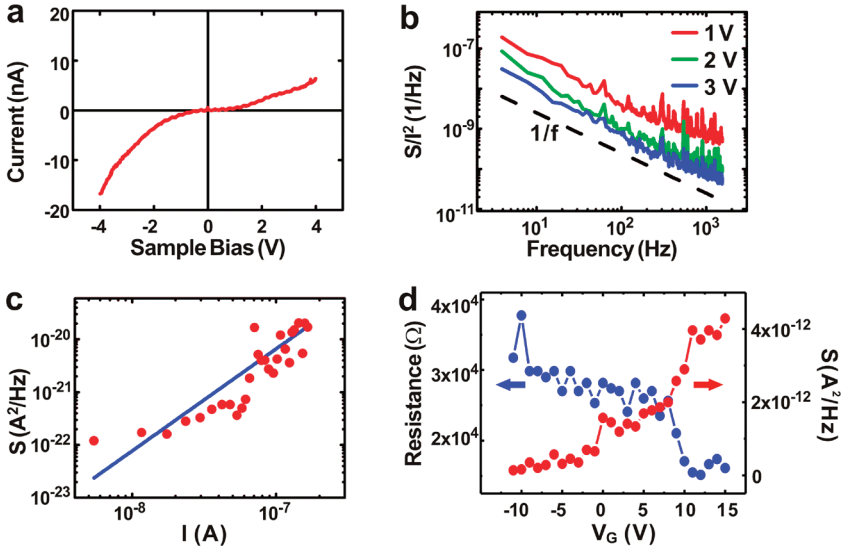

Figure 3. Conducting AFM analysis on graphene strips: (a) $I-V$ curves measured on graphene patterns; (b) normalized PSD measured on graphene patterns. Note that the normalized PSD was proportional to the inverse of frequency, indicating the 1/f noise behavior; (c) PSD S *versus* current I. Here, the S and I values were measured while changing the sample bias voltages from 0.1 to 2.9 V. The graph can be fitted by the curve of $S \approx I^{1.9}$, which is also a typical behavior of 1/f noise; (d) graph showing resistance and PSD S at different gate bias voltages on the graphene strip. The drain-source bias V_{ds} was 1 V. The PSD of the patterned graphene shows an opposite tendency with resistance change.

The electrical and noise characteristics of a graphene strip were analyzed using the SNM (Figure 3). Figure 3a shows a typical $I-V$ curve measured at the fixed position of the graphene strip surface. In this case, the channel length and width of the graphene strip were ~20 and 6.6 μm, respectively. For the measurement, the bias voltage was applied to the Au electrode, and the currents were measured using the conducting AFM. The $I-V$ characteristics showed a nonlinear behavior. This nonlinearity suggested a Schottky barrier between the Pt tip and the graphene strip.

Figure 3b shows the normalized PSD S/I^2 of the graphene strip at different sample bias voltages. Here, the current PSD (up to 1 kHz) was measured by the network analyzer with different sample bias voltages. In the low-frequency region, the normalized PSD varied as $f^{-\beta}$, where β was estimated as 1.07 ± 0.04 by fitting each spectrum. This result showed that our graphene strip had a typical 1/f noise behavior.

Figure 3c shows the graph of the PSD S *versus* current I. In this experiment, the current PSD was measured at the frequency of 3.9 Hz for different sample currents. The sample current was controlled by changing the sample bias voltages. The measured PSD (red dots) *versus* currents was plotted in a log−log scale and fitted with $S \approx I^n$ (a blue line), where n was estimated as ~1.9 when a positive bias was applied onto the graphene. We also performed a similar experiment with a negative bias voltage onto the graphene and obtained a similar result (Figure S2 in Supporting Information). Previous works show that

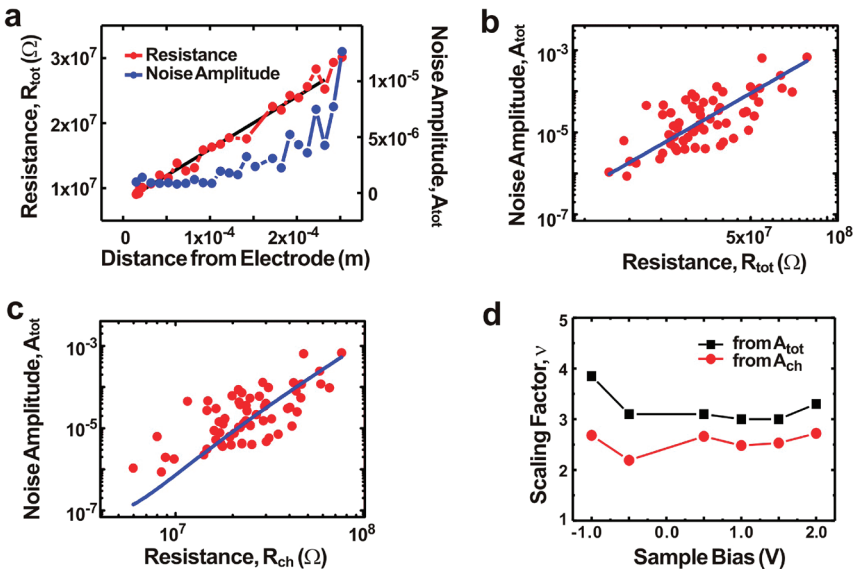

Figure 4. Scanning noise analysis on graphene strips. The back-gate voltage was fixed at 0 V. (a) Resistance R_{tot} and noise amplitude A_{tot} of a typical graphene strip with different distances between the tip and the Au electrode. The resistance graph was fitted by the black line based on $R_{tot} = \rho_{ch}L/a + C$, where ρ_{ch} is 3.5 $\times$ 10^{-3} Ωm and C is 7.9 $\times$ 10^6 Ω. (b) Noise amplitude A_{tot} at different total resistance R_{tot} including those of the graphene strip channel and contacts. The data were obtained from panel a. The blue line represents the fitting curve based on $A_{tot} \propto R_{tot}^{\nu}$, where ν is 3.5. (c) Noise amplitude A_{tot} at different graphene strip channel resistance R_{ch}. The blue line represents fitting results based on $A_{tot} = [\alpha \times R_{ch}^{\nu} \cdot R_{ch}^2 + D]/(R_{ch} + C)^2$, where α and ν were 5.1 $\times$ 10^{-26} $\Omega^{-2.8}$ and 2.8, respectively. C and D are fitting parameters representing the noise characteristics of the electrode-graphene or tip-graphene contacts. (d) Estimated scaling factors with different sample bias voltages.

the 1/*f* noise can be written as[52−54]

$$S = A\frac{I^2}{f} \qquad (1)$$

where *A* and *f* represent a noise amplitude and a frequency, respectively. From this result, we confirmed that our graphene strip also followed eq 1 for a typical behavior of 1/*f* noise. It also should be noted that the scaling factor *n* may vary depending on the applied bias voltages, and one can analyze the measured noise data as a 1/*f* noise only in the bias voltage range where the scaling factor *n* is close to 2.[52−54] Our measurement shows the scaling factor *n* was close to 2 in the bias voltage range of −1.5 to 2.9 V (Figure 3c and Figure S2 in Supporting Information), indicating that we can perform the noise analysis of the graphene strip assuming a 1/*f* noise in this bias voltage range.

The representative measured resistance (red dots) and current PSD (at 3.9 Hz) (blue dots) *versus* back-gate voltages are shown in Figure 3d. In this experiment, the sample bias of 1 V was applied between the electrode and Pt tip, and the sample current and current PSD were measured with different gate bias voltages applied on the underlying highly doped Si substrates. Note that the resistance and the PSD had an opposite tendency. This behavior is the typical characteristics of multilayer graphene.[55,56]

The scaling behaviors of the noise characteristics of graphene strips were analyzed by SNM (Figure 4). In this experiment, the Pt tip was placed on different locations of the graphene strip, and the electrical currents and the current PSD were measured. Then, the resistance R_{tot} and the noise amplitude A_{tot} at each location were estimated from the measured current and PSD values. Note that the measured noise characteristics included not only the noise information of the graphene strip-based device but also that of the contact between Pt tip and the Au electrode. Therefore, we developed an empirical model to extract the noise characteristics of only the graphene strip channel (Figure S3 in the Supporting Information).

As a first step, we applied an empirical model to the measured resistance data to extract the resistance values of only the graphene strip channels. The measured resistance R_{tot} can be written as the sum of R_{tip} (the contact resistance between the Pt tip and the graphene strip), R_{ch} (the resistance of the graphene strip), and R_{elec} (the contact resistance between the Au electrode and the graphene strip) like,

$$R_{tot} = R_{ch} + R_{elec} + R_{tip} = \frac{\rho_{ch}}{a}L + C \qquad (2)$$

where ρ_{ch}, L, and a represent the resistivity of the graphene strip, a distance from the Au electrode to the Pt tip, and the cross section area of the graphene strip, respectively. Here, $(\rho_{ch}/a)L$ represents the channel resistance R_{ch}, and C is defined as the sum of R_{tip} and R_{elec}. For a uniform graphene strip, we can assume that ρ_{ch}/a is a constant. Furthermore, since we utilized the same Pt tip to measure the resistance and the noise characteristics on different locations of the graphene

strip channel, we can assume that the contact resistance C was constant. In this case, the channel resistance R_{ch} (=(ρ_{ch}/a)L) at each measurement location can be obtained by fitting the measured resistance R_{tot} using eq 2.

As a next step, we developed an empirical model to obtain the noise amplitude A_{ch} of the graphene strip channel from the measured total noise amplitude A_{tot}. The total noise amplitude A_{tot} measured in the SNM experiment can be expressed by the noise amplitude values of individual resistance parts in the current path like,[57]

$$\begin{aligned} A_{tot} &= [A_{ch}R_{ch}^2 + A_{elec}R_{elec}^2 + A_{tip}R_{tip}^2]/R_{tot}^2 \\ &= [A_{ch}R_{ch}^2 + D]/(R_{ch}+C)^2 \end{aligned} \quad (3)$$

where A_{ch}, A_{cont}, and A_{tip} represent the noise amplitude of the resistance parts in the graphene strip channel, the Au electrode contact, and the Pt tip, respectively. D is defined as $A_{elec}R_{elec}^2 + A_{tip}R_{tip}^2$, representing the noise from the Au electrodes and the Pt tip. Since we utilized the same Pt tip for entire SNM experiment, we can assume that D remained constant during our measurement. Finally, if we assumed a general power law $A_{ch} \cong \alpha \times R_{ch}^{\nu}$ regarding the noise from the graphene strip,[57] eq 3 can be written as

$$A_{tot} = [(\alpha \cdot R_{ch}^{\nu}) \cdot R_{ch}^2 + D]/(R_{ch}+C)^2 \quad (4)$$

where the α and ν are the coefficient and the scaling factor of the channel resistance, respectively. Thus, the characteristic parameters (α and ν) of the noise from the graphene strip channel can be obtained by fitting the graph of the measured A_{tot} *versus* the estimated R_{ch} using eq 4 (Figure S3 in the Supporting Information).[57−64]

Figure 4a shows the resistance R_{tot} (red dot) and the noise amplitude A_{tot} (blue dot) measured when the Pt tip was placed on the graphene strip surface with a distance L from the Au electrode. For the measurement, the sample bias of 2 V was applied to the Au electrode of the sample. The resistance and the noise of the graphene strip (width $\approx$ 6.6 μm) were measured after locating the probe at six different positions with the distances of $\pm$1.5, $\pm$ 0.9, and $\pm$0.3 μm from its center along the width direction, and the measured values were averaged to obtain each data point in Figure 4a. Note that the measured total resistance R_{tot} was linearly proportional to the distance L, which supports that both ρ_{ch}/a and C in eq 2 can be considered as a constant in our system. The measured resistance R_{tot} graph was fitted using eq 2 to obtain the channel resistance values R_{ch} (= (ρ_{ch}/a)L) at each measurement location.

One important issue in this measurement can be that our conducting probe made a *point* contact with the *wide* graphene strip, which might cause some deviation in the relationship between the resistance R_{tot} and the channel length L of the graphene strip. To estimate the effect of the point tip contact, we performed a finite element method simulation and calculated the relationship of R_{tot} *versus* L with a point contact probe (Figure S4 in Supporting Information). The simulation results show that the R_{tot} values measured with a point contact probe are *linearly proportional* to L if L is much larger than the width W of the graphene strip. Since we performed our SNM measurement by placing the probe mostly at the positions with L values much larger than the graphene strip width of $\sim$6.6 μm, the effect of *point* contacts on the results in Figure 4a should be minimal.

Figure 4b shows the graph of the total noise amplitude A_{tot} *versus* the total resistance R_{tot}. This graph was plotted using the data in Figure 4a. The data can be fitted by the typical power law $A_{tot} \propto R_{tot}^{\nu}$, which resulted in the scaling parameter of $\nu \approx 3.5$. It is a bit larger than previous analysis results of $\sim$3.2 measured from multiple devices.[39] Presumably, it is because the noise amplitude A_{tot} and the resistance R_{tot} include the contribution from the contact between the graphene and the Pt tip as well as the graphene channel.

The scaling behavior of the noise only from the graphene strip channel can be obtained by fitting the data in Figure 4a using the empirical model as explained before (Figure 4c). In brief, we first fit the graph of the total resistance R_{tot} in Figure 4a by eq 2 to obtain the graphene channel resistance R_{ch} at each location on the graphene strip. Then, the graph of the total noise amplitude A_{tot} was fitted using eq 4, and the estimated channel resistance R_{ch} (Figure 4c). The estimated parameters α and ν are 5.1 $\times$ 10^{-26} and 2.8, respectively. Thus, the scaling behavior of the graphene channel noise can be written as

$$A_{ch} \cong 5.1 \times 10^{-26} R_{ch}^{2.8} \quad (5)$$

The scaling factor 2.8 is smaller than previous results obtained using multiple graphene devices with different resistance values.[39] It implies that the noise amplitude is rather sensitive to the contact problem as well as the defects in the graphene strip channel. We also prepared multiple graphene channel devices with different resistance values and performed a noise analysis similar to previous works, obtaining a similar scaling factor of $\sim$2.6 (Figure S5 in Supporting Information). Note that unlike previous noise analysis methods, our SNM method allows us to perform noise analysis using only a single graphene channel device, which should make it a powerful strategy for basic device researches and applications.

Figure 4d shows the scaling factors of the graphene channel noise with different sample bias voltages. Here, we applied the different sample bias voltages of $-$1.0 to 2.0 V to the Au electrode and performed the similar noise analysis regarding the scaling behavior of

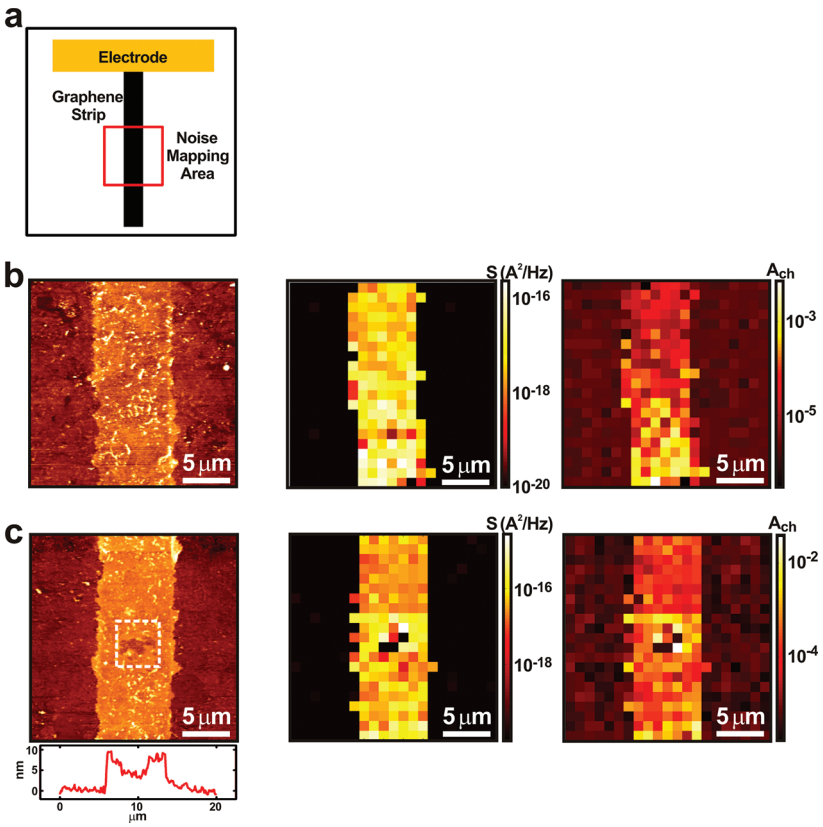

Figure 5. Scanning noise mapping using the scanning noise microscopy. (a) Schematic diagram showing the structure of our graphene sample and imaged surface area on it. (b) AFM topography image (i) of a typical graphene strip without defects, and the map of the noise PSD data (ii) and the channel noise amplitude A_{ch} (iii) from the graphene strip. The bright area represents the graphene strip regions. Note that the channel noise amplitude A_{ch} increased as the conducting tip moved away from the electrode. (c) AFM topography image (i) of a graphene strip with a defect in the middle, and the map of the noise PSD data (ii) and the channel noise amplitude A_{ch} (iii) from the graphene strip. The bright area represents the graphene strip region. It shows the enhanced channel noise amplitude A_{ch} near the defect of the graphene strip.

the graphene channel noise. *Black* and *red* dots represent the scaling factor estimated from the *total noise amplitude* and the *channel noise amplitude* of the graphene strip devices, respectively. The scaling factor estimated from the channel noise amplitude of the graphene strip did not vary much with its average of 2.54 even under different bias voltages. It also should be noted that the tip used for the measurement under the *negative* bias was different from that used under the *positive* bias and even resulted in different current levels due to their different contact resistances (Figure 3c and Figure S2 in Supporting Information). However, we could obtain similar values for the scaling factor ν after our noise analysis. This result clearly shows our method can remove the effect of different contact resistances and enable the reliable noise analysis of graphene strips.

The SNM method allows us to obtain two-dimensional mapping of noise characteristics on a graphene-device (Figure 5). In this experiment, we measured the noise characteristics after placing the Pt tip on different locations in the graphene strip region (marked by a red square) of the device (Figure 5a). The measurement results on a pristine graphene strip are shown in Figure 5b. The *left* and the *middle* images are the AFM topography and the noise PSD map of the graphene strip (brighter regions) on the SiO_2 substrate (darker regions), respectively. The Au electrode was connected to the graphene strip from the upper part of the image as depicted in Figure 5a. Note that the PSD signal was observed only on the graphene regions because the current flows only on the graphene regions. The right image of Figure 5b shows the map of the channel noise amplitude A_{ch} which was estimated using our empirical model as explained in Figure 4. Note that A_{ch} in the lower part of the image appeared larger than that on the upper part. It is because the Au electrode was connected to the graphene strip from the upper part of the image and the graphene channel resistance increased as the Pt tip moved away from the Au electrode. It is also worth mentioning that the variations of the noise amplitude and the resistance along the width direction of the graphene strip were rather small (Figure 5b and Figure S6 in Supporting Information). When we estimated the scaling factor ν eq 4 using the data at the different positions along the width direction in Figure 5b, it ranged between 2.48 and 2.75. These values are

consistent with that in eq 5. It implies that the effect of contact position along the width direction is minimal in our noise analysis shown in Figure 4.

The capability of two-dimensional mapping of noises can provide versatile information of nanoscale devices. As a proof of concepts, we performed the noise mapping experiment on the same graphene strip in Figure 5b after creating a defect on it (Figure 5c). Here, the defect was created by scratching the graphene strip using a rather hard AFM tip (spring constant of 18 N/m). The AFM topography image shows the defect with the depth of ~3 nm and the width of ~3 μm (left of Figure 5c). The map of the noise PSD (middle) and the channel noise amplitude (right) clearly show the increased noise around the defect (Figure 5c). Since our SNM system is relying on a CAFM probe, its resolution should be determined by the sizes of CAFM probes and imaging pixels just like a CAFM system. Previous report shows that the resolution of a CAFM can be as small as ~1 nm.[6] As an example of a high-resolution SNM imaging, we demonstrated the SNM imaging of single-walled carbon nanotubes (Figure S7 in Supporting Information). This result clearly shows the potential of our SNM method as a versatile tool for nanoscale noise analysis for nanodevice research.

CONCLUSIONS

We developed the SNM method for the nanoscale noise analysis of nanodevices and successfully demonstrated the noise analysis of a graphene strip using this method. The SNM method allowed us to measure the noise scaling behavior of the graphene strip using a single sample. The obtained noise scaling factor of the graphene strip was well consistent with the previous result measured using multiple devices. Furthermore, the nanoscale noise map of a graphene strip was successfully obtained, which allowed us to study the effect of structural defect on the noise in graphene strip channel. The SNM is a simple but versatile technique, and it should provide a tremendous flexibility for the noise analysis of nanoscale devices.

METHODS

Fabrication Method for Graphene Strip Devices. First, a graphene sheet grown by the chemical vapor deposition method was transferred onto a clean SiO_2 substrate (oxide thickness ≈ 1000 Å). Then a Ti/Au (100/300 Å) electrode was fabricated on the graphene substrate *via* thermal evaporation through a shadow mask. Next, using a conventional photolithography method, photoresist (PR) was patterned on the graphene surface. Conducting polymer, polypyrrole films were synthesized from the mixture of 0.1 M pyrrole and 0.1 M sodium chloride in an aqueous solution at +0.8 V (*vs* an Ag/AgCl reference electrode) using the electrochemical deposition method.[65,66] The total polymerization charge was 150 mC. Note that the photoresist pattern was utilized as a passivation layer, and therefore polypyrrole films were deposited only on the uncovered graphene surface. After the deposition of polypyrrole films, PR was removed with acetone, leaving only polypyrrole patterns on the graphene surface. Then, the substrate was stirred in deionized water using a vortexer (IKA, Minishaker MS2) at 2500 rpm for 1 min. Because of the swirling flow of deionized water, the conducting polymer and the underlying graphene strip were mechanically detached off from the substrate, leaving graphene strip patterns.

Acknowledgment. This work was supported by the NRF Grant 2011-0000390 and the Conversing Research Center Program (2011K000683). S.H. acknowledges the support from the WCU program (R31-10032) and the NBIT program (2011-00240).

Supporting Information Available: Supplementary fitting methods and supplementary figures. This material is available free of charge *via* the Internet at http://pubs.acs.org.

REFERENCES AND NOTES

1. Hansma, P. K.; Elings, V. B.; Marti, O.; Bracker, C. E. Scanning Tunneling Microscopy and Atomic Force Microscopy—Application to Biology and Technology. *Science* **1988**, *242*, 209–216.
2. Kim, Y.; Lieber, C. M. Machining Oxide Thin-Films with an Atomic Force Microscope—Pattern and Object Formation on the Nanometer Scale. *Science* **1992**, *257*, 375–377.
3. Meyer, E.; Glatzel, T. Novel Probes for Molecular Electronics. *Science* **2009**, *324*, 1397–1398.
4. Cook, R. F. Probing the Nanoscale. *Science* **2010**, *328*, 183–184.
5. Shekhawat, G. S.; Dravid, V. P. Nanoscale Imaging of Buried Structures *via* Scanning Near-Field Ultrasound Holography. *Science* **2005**, *310*, 89–92.
6. Scaini, D.; Castronovo, M.; Casalis, L.; Scoles, G. Electron Transfer Mediating Properties of Hydrocarbons as a Function of Chain Length: A Differential Scanning Conductive Tip Atomic Force Microscopy Investigation. *ACS Nano* **2008**, *2*, 507–515.
7. Yakuphanoglu, F.; Okur, S. Analysis of Electronic Parameters and Interface States of Boron Dispersed Triethanolamine/P-Si Structure by AFM, I-V, C-V-F and G/Omega-V-F Techniques. *Microelectron. Eng.* **2010**, *87*, 30–34.
8. Chung, J. W.; Yang, H.; Singh, B.; Moon, H.; An, B. K.; Lee, S. Y.; Park, S. Y. Single-Crystalline Organic Nanowires with Large Mobility and Strong Fluorescence Emission: A Conductive-AFM and Space-Charge-Limited-Current Study. *J. Mater. Chem.* **2009**, *19*, 5920–5925.
9. Cohen, H.; Nogues, C.; Naaman, R.; Porath, D. Direct Measurement of Electrical Transport through Single DNA Molecules of Complex Sequence. *Proc. Natl. Acad. Sci. U.S.A.* **2005**, *102*, 11589–11593.
10. Liu, K.; Wang, X. H.; Wang, F. S. Probing Charge Transport of Ruthenium-Complex-Based Molecular Wires at the Single-Molecule Level. *ACS Nano* **2008**, *2*, 2315–2323.
11. Nonnenmacher, M.; Oboyle, M. P.; Wickramasinghe, H. K. Kelvin Probe Force Microscopy. *Appl. Phys. Lett.* **1991**, *58*, 2921–2923.
12. Kikukawa, A.; Hosaka, S.; Imura, R. Silicon PN Junction Imaging and Characterizations Using Sensitivity Enhanced Kelvin Probe Force Microscopy. *Appl. Phys. Lett.* **1995**, *66*, 3510–3512.
13. Hoppe, H.; Glatzel, T.; Niggemann, M.; Hinsch, A.; Lux-Steiner, M. C.; Sariciftci, N. S. Kelvin Probe Force Microscopy Study on Conjugated Polymer/Fullerene Bulk Heterojunction Organic Solar Cells. *Nano Lett.* **2005**, *5*, 269–274.
14. Xu, B. Q.; Tao, N. J. J. Measurement of Single-Molecule Resistance by Repeated Formation of Molecular Junctions. *Science* **2003**, *301*, 1221–1223.

15. Puntambekar, K. P.; Pesavento, P. V.; Frisbie, C. D. Surface Potential Profiling and Contact Resistance Measurements on Operating Pentacene Thin-Film Transistors by Kelvin Probe Force Microscopy. *Appl. Phys. Lett.* **2003**, *83*, 5539–5541.
16. Hossain, M. Z.; Rumyantsev, S. L.; Shahil, K. M. F.; Teweldebrhan, D.; Shur, M.; Balandin, A. A. Low-Frequency Current Fluctuations in "Graphene-like" Exfoliated Thin-Films of Bismuth Selenide Topological Insulators. *ACS Nano* **2011**, *5*, 2657–2663.
17. Hossain, M. Z.; Rumyantsev, S. L.; Teweldebrhan, D.; Shahil, K. M. F.; Shur, M.; Balandin, A. A. 1/*f* Noise in Conducting Channels of Topological Insulator Materials. *Phys. Status Solidi A* **2011**, *208*, 144–146.
18. Chung, Y.; Song, S. H. Implementation of Low-Voltage Static RAM with Enhanced Data Stability and Circuit Speed. *Microelectron. J.* **2009**, *40*, 944–951.
19. Calhoun, B. H.; Chandrakasan, A. P. Static Noise Margin Variation for Sub-Threshold SRAM in 65-nm CMOS. *IEEE J. Solid-State Circ.* **2006**, *41*, 1673–1679.
20. Wellig, A.; Zory, J. Static Noise Margin Analysis of Sub-Threshold SRAM Cells in Deep Sub-Micron Technology. *Lect. Notes Comput. Sci.* **2005**, *3728*, 488–497.
21. Liu, G.; Stillman, W.; Rumyantsev, S.; Shao, Q.; Shur, M.; Balandin, A. A. Low-Frequency Electronic Noise in the Double-Gate Single-Layer Graphene Transistors. *Appl. Phys. Lett.* **2009**, *95*, 033103.
22. Shao, Q. H.; Liu, G. X.; Teweldebrhan, D.; Balandin, A. A.; Runryantsev, S.; Shur, M. S.; Yan, D. Flicker Noise in Bilayer Graphene Transistors. *IEEE Electr. Device. Lett.* **2009**, *30*, 288–290.
23. Rumyantsev, S.; Liu, G.; Stillman, W.; Shur, M.; Balandin, A. A. Electrical and Noise Characteristics of Graphene Field-Effect Transistors: Ambient Effects, Noise Sources and Physical Mechanisms. *J. Phys. Condens. Matter* **2010**, *22*, 395302.
24. Xu, G. Y.; Torres, C. M.; Zhang, Y. G.; Liu, F.; Song, E. B.; Wang, M. S.; Zhou, Y.; Zeng, C. F.; Wang, K. L. Effect of Spatial Charge Inhomogeneity on 1/*f* Noise Behavior in Graphene. *Nano Lett.* **2010**, *10*, 3312–3317.
25. Cheng, Z. G.; Li, Q.; Li, Z. J.; Zhou, Q. Y.; Fang, Y. Suspended Graphene Sensors with Improved Signal and Reduced Noise. *Nano Lett.* **2010**, *10*, 1864–1868.
26. Lin, Y. M.; Avouris, P. Strong Suppression of Electrical Noise in Bilayer Graphene Nanodevices. *Nano Lett.* **2008**, *8*, 2119–2125.
27. Xu, G. Y.; Torres, C. M.; Tang, J. S.; Bai, J. W.; Song, E. B.; Huang, Y.; Duan, X. F.; Zhang, Y. G.; Wang, K. L. Edge Effect on Resistance Scaling Rules in Graphene Nanostructures. *Nano Lett.* **2011**, *11*, 1082–1086.
28. Xu, G. Y.; Torres, C. M.; Song, E. B.; Tang, J. S.; Bai, J. W.; Duan, X. F.; Zhang, Y. G.; Wang, K. L. Enhanced Conductance Fluctuation by Quantum Confinement Effect in Graphene Nanoribbons. *Nano Lett.* **2010**, *10*, 4590–4594.
29. Snow, E. S.; Novak, J. P.; Lay, M. D.; Perkins, F. K. 1/*f* Noise in Single-Walled Carbon Nanotube Devices. *Appl. Phys. Lett.* **2004**, *85*, 4172–4174.
30. Collins, P. G.; Fuhrer, M. S.; Zettl, A. 1/*f* Noise in Carbon Nanotubes. *Appl. Phys. Lett.* **2000**, *76*, 894–896.
31. Gomez-Navarro, C.; De Pablo, P. J.; Gomez-Herrero, J.; Biel, B.; Garcia-Vidal, F. J.; Rubio, A.; Flores, F. Tuning the Conductance of Single-Walled Carbon Nanotubes by Ion Irradiation in the Anderson Localization Regime. *Nat. Mater.* **2005**, *4*, 534–539.
32. Lee, J. W.; Jang, D.; Kim, G. T.; Mouis, M.; Ghibaudo, G. Analysis of Charge Sensitivity and Low Frequency Noise Limitation in Silicon Nanowire Sensors. *J. Appl. Phys.* **2010**, *107*.
33. Wang, W. Y.; Xiong, H. D.; Edelstein, M. D.; Gundlach, D.; Suehle, J. S.; Richter, C. A.; Hong, W. K.; Lee, T. Low Frequency Noise Characterizations of ZnO Nanowire Field Effect Transistors. *J. Appl. Phys.* **2007**, *101*.
34. Cheng, Z. G.; Li, Q.; Li, Z. J.; Zhou, Q. Y.; Fang, Y. Suspended Graphene Sensors with Improved Signal and Reduced Noise. *Nano Lett.* **2010**, *10*, 1864–1868.
35. Zhuge, J.; Wang, R. S.; Huang, R.; Tian, Y.; Zhang, L. L.; Kim, D. W.; Park, D.; Wang, Y. Y. Investigation of Low-Frequency Noise in Silicon Nanowire MOSFETs. *IEEE Electr. Device. Lett.* **2009**, *30*, 57–60.
36. Choi, S. H.; Yee, S. M.; Ji, H. J.; Choi, J. W.; Cho, Y. S.; Kim, G. T. Smart Gas Sensor and Noise Properties of Single ZnO Nanowire. *Jpn. J. Appl. Phys.* **2009**, *48*.
37. Zhou, C. G.; Zhang, X. G. Numerical Study of the Noise Power of a Carbon Nanowire Network. *Phys. Rev. B* **2008**, *78*.
38. Liu, F.; Wang, K. L. Correlated Random Telegraph Signal and Low-Frequency Noise in Carbon Nanotube Transistors. *Nano Lett.* **2008**, *8*, 147–151.
39. Kim, K.; Park, H. J.; Woo, B. C.; Kim, K. J.; Kim, G. T.; Yun, W. S. Electric Property Evolution of Structurally Defected Multilayer Graphene. *Nano Lett.* **2008**, *8*, 3092–3096.
40. Back, J. H.; Kim, S.; Mohammadi, S.; Shim, M. Low-Frequency Noise in Ambipolar Carbon Nanotube Transistors. *Nano Lett.* **2008**, *8*, 1090–1094.
41. Pal, A. N.; Ghosh, A. Resistance Noise in Electrically Biased Bilayer Graphene. *Phys. Rev. Lett.* **2009**, *102*.
42. Li, X. S.; Zhu, Y. W.; Cai, W. W.; Borysiak, M.; Han, B. Y.; Chen, D.; Piner, R. D.; Colombo, L.; Ruoff, R. S. Transfer of Large-Area Graphene Films for High-Performance Transparent Conductive Electrodes. *Nano Lett.* **2009**, *9*, 4359–4363.
43. Reina, A.; Jia, X. T.; Ho, J.; Nezich, D.; Son, H. B.; Bulovic, V.; Dresselhaus, M. S.; Kong, J. Layer Area, Few-Layer Graphene Films on Arbitrary Substrates by Chemical Vapor Deposition. *Nano Lett.* **2009**, *9*, 3087–3087.
44. Lorenz, H.; Despont, M.; Fahrni, N.; Brugger, J.; Vettiger, P.; Renaud, P. High-Aspect-Ratio, Ultrathick, Negative-Tone Near-UV Photoresist and Its Applications for MEMS. *Sens. Actuators A* **1998**, *64*, 33–39.
45. Lee, K. Y.; LaBianca, N.; Rishton, S. A.; Zolgharnain, S.; Gelorme, J. D.; Shaw, J.; Chang, T. H. P. Micromachining Applications of a High Resolution Ultra-thick Photoresist. *J Vac. Sci. Technol. B* **1995**, *13*, 3012–3016.
46. Yeo, B. S.; Stadler, J.; Schmid, T.; Zenobi, R.; Zhang, W. H. Tip-Enhanced Raman Spectroscopy—Its Status, Challenges and Future Directions. *Chem. Phys. Lett.* **2009**, *472*, 1–13.
47. Yamamoto, T.; Suzuki, Y.; Miyashita, M.; Sugimura, H.; Nakagiri, N. Development of a Metal Patterned Cantilever for Scanning Capacitance Microscopy and Its Application to the Observation of Semiconductor Devices. *J. Vac. Sci. Technol. B* **1997**, *15*, 1547–1550.
48. Ross, M. F.; Comfort, D.; Gorin, G. Plasma Etch Characteristics of Electron-Beam Processed Photoresist. *Proc. SPIE* **1995**, *2438*, 803.
49. Lo, B.; Tai, C. C.; Chang, J. Y.; Wu, C. H.; Chen, B. J.; Kuo, T. C.; Lian, P. J.; Ling, Y. C. Supercritical Carbon Dioxide-Assisted Oxidative Degradation and Removal of Polymer Residue after Reactive Ion Etching of Photoresist. *Green Chem.* **2007**, *9*, 133–138.
50. Kim, H. J.; Kim, D. J.; Ryu, J. K.; Pak, S. S. Removal of the Photoresist (PR) and Metallic-Polymer in the Concave-Typed Storage Node Using the Excimer Laser. *Appl. Surf. Sci.* **2004**, *228*, 100–109.
51. Makoto, S.; Touno, I.; Omiya, K.; Homma, T.; Nagatomo, T. A Process for Photoresist Removal after Aluminum Etching Using Plasma Treatment in a Gas Containing Hydrogen. *J. Electrochem. Soc.* **2002**, *149*, G451–G454.
52. Hooge, F. N. 1/*f* Noises. *Phys. A* **1976**, *83B*, 14.
53. Hooge, F. N.; Kleinpenning, T. G. M.; Vandamme, L. K. J. Experimental Studies on 1-F Noise. *Rep. Prog. Phys.* **1981**, *4*, 479–532.
54. Dutta, P.; Horn, P. M. Low-Frequency Fluctuations in Solids—1-F Noise. *Rev. Mod. Phys.* **1981**, *53*, 497–516.
55. Pal, A. N.; Ghosh, A. Ultralow Noise Field-Effect Transistor from Multilayer Graphene. *Appl. Phys. Lett.* **2009**, *95*, 082105.
56. Novoselov, K. S.; Geim, A. K.; Morozov, S. V.; Jiang, D.; Zhang, Y.; Dubonos, S. V.; G., IV; Firsov, A. A. Electric Field Effect in Atomically Thin Carbon Films. *Science* **2004**, *306*, 666–669.

57. Lee, H.; Lee, M.; Namgung, S.; Hong, S. Wide Contact Structures for Low-Noise Nanochannel Devices Based on a Carbon Nanotube Network. *ACS Nano* **2010**, *4*, 7612–7618.
58. Breeze, A. J.; Carter, S. A.; Alers, G. B.; Heaney, M. B. 1/f Noise Through the Metal-Nonmetal Transition in Percolating Composites. *Appl. Phys. Lett.* **2000**, *76*, 592–594.
59. Golden, K. M. Critical Behavior of Transport in Lattice and Continuum Percolation Models. *Phys. Rev. Lett.* **1997**, *78*, 3935–3938.
60. Tremblay, A. -M. S.; Feng, S.; Breton, P. Exponents for 1/f Noise Near a Continuum Percolation-Threshold. *Phys. Rev. B* **1986**, *33*, 2077–2080.
61. Rammal, R.; Tannous, C.; Breton, P.; Tremblay, A. M. S. Flicker (1-f) Noise in Percolation Networks—A New Hierarchy of Exponents. *Phys. Rev. Lett.* **1985**, *54*, 1718–1721.
62. Mantese, J. V.; Webb, W. W. 1/f Noise of Granular Metal-Insulator Composites. *Phys. Rev. Lett.* **1985**, *55*, 2212–2215.
63. Koch, R. H.; Laibowitz, R. B.; Alessandrini, E. I.; Viggiano, J. M. Resistivity-Noise Measurements in Thin Gold-Films Near the Percolation-Threshold. *Phys. Rev. B* **1985**, *32*, 6932–6935.
64. Chen, C. C.; Chou, Y. C. Electrical-Conductivity Fluctuations Near the Percolation-Threshold. *Phys. Rev. Lett.* **1985**, *54*, 2529–2532.
65. Mangold, K. M.; Schafer, S.; Juttner, K. Reference Electrodes based on Conducting Polymers. *Fresen. J. Anal. Chem.* **2000**, *367*, 340–342.
66. Grzeszczuk, M.; Kepas, A.; Zabinska-Olszak, G. Electrochemical Preparation and Redox/Ion Exchange Properties of Polypyrrole in Aqueous Sodium Hexafluoroaluminate. *Electrochim. Acta* **2004**, *49*, 2405–2414.